Volume Measurements of Normal Orbital Structures by Computed Tomographic Analysis

Glenn Forbes, Dale G. Gehring, Colum A. Gorman, Michael D. Brennan and Ian T. Jackson

AJNR Am J Neuroradiol 1985, 6 (3) 419-424
http://www.ajnr.org/content/6/3/419

Volume Measurements of Normal Orbital Structures by Computed Tomographic Analysis

Glenn Forbes[1]
Dale G. Gehring[1]
Colum A. Gorman[2]
Michael D. Brennan[2]
Ian T. Jackson[3]

Computed tomographic digital data and special off-line computer graphic analysis were used to measure volumes of normal orbital soft tissue, extraocular muscle, orbital fat, and total bony orbit in vivo in 29 patients (58 orbits). The upper limits of normal for adult bony orbit, soft tissue exclusive of the globe, orbital fat, and muscle are 30.1 cm^3, 20.0 cm^3, 14.4 cm^3, and 6.5 cm^3, respectively. There are small differences in men as a group compared with women but minimal difference between right and left orbits in the same person. The accuracy of the techniques was established at 7%–8% for these orbit structural volumes in physical phantoms and in simulated silicone orbit phantoms in dry skulls. Mean values and upper limits of normal for volumes were determined in adult orbital structures for future comparison with changes due to endocrine ophthalmopathy, trauma, and congenital deformity.

Late-generation computed tomographic (CT) scanners can demonstrate small differences of contrast (density) even in small structures (1–2 mm). Although the absolute density measurements are seldom reliable enough to offer significant specificity [1], the relative differences are sufficiently consistent to provide reproducible boundaries for image display and volume determination. Summation of pixel counts in successive cross-sectional areas based on density ranges can provide volume measurements of three-dimensional structures [2, 3]. Brenner et al. [4], using 10-mm slice widths and 1-cm intervals, reported 10% accuracy of calculated CT volumes of large viscera correlated with cadaver measurements. Heymsfield et al. [5] showed 5% accuracy of direct cadaver organ CT volume measurements. Similar measurements have been performed on dog organs with commercially available CT scanners and off-line analysis [6]. Recently, Forbes et al. [7] described pilot studies with special off-line computer programs to measure small-structure volumes in the orbit. If thin slices (1.5 mm) and high contrast differences for boundary display are used, measurements accurate within 1%–7% are achieved for volume determinations in the range of 4–60 cm^3 in physical phantoms, depending on technique and specific structural volume.

Although these techniques can be used in any area of the body, the orbit is an excellent subject for computerized volume study for several reasons. Marked differences in contrast exist among the intraorbital structures, which consist of fat, muscle, fluid (in the globe), air (in adjacent sinuses), and bone, that minimize the overlap of density ranges for determining boundaries. Furthermore, no comprehensive normal in vivo volume studies of the different orbital components with documentation of the accuracy of the techniques have been attempted. Previous attempts at orbital volume determinations have been limited to in vitro animal studies, dry-skull human studies, and in vivo estimates of total bony orbit volume from linear radiographic measurements without regard to soft-tissue components. And finally, for future work, different variants of Graves disease produce a wide variation of volume changes in the orbit muscle and fat that have not yet been classified [8–13].

This article appears in the May/June 1985 issue of *AJNR* and the July 1985 issue of *AJR*.

Received March 28, 1984; accepted after revision October 10, 1984.

[1] Department of Diagnostic Radiology, Mayo Clinic and Mayo Foundation, Rochester, MN 55905. Address reprint requests to G. Forbes.

[2] Division of Endocrinology, Metabolism and Internal Medicine, Mayo Clinic and Mayo Foundation, Rochester, MN 55905.

[3] Section of Plastic and Reconstructive Surgery, Mayo Clinic and Mayo Foundation, Rochester, MN 55905.

***AJNR* 6:419–424, May/June 1985**
0195–6108/85/0603–0419

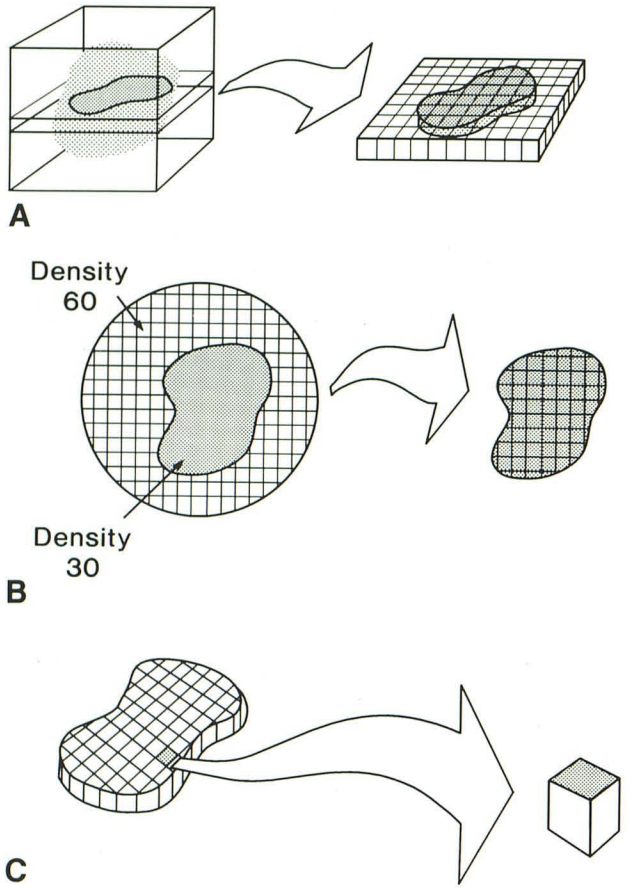

Fig. 1.—**A**, CT digital data acquisition. Continuous and contiguous thin slices through three-dimensional structure provide series of planes for pixel counting. **B**, Pixel counting. Pixels representing structure of interest are differentiated from other areas through predetermined range of attenuation density. Pixels contiguous with starting point ("seed point") and falling within prescribed density range are selectively counted ("neighborhood-sampling," "region-growing" techniques). **C**, Voxel calibration. Each pixel count represents three-dimensional voxel of measurable volume determined by matrix size and scanner configuration. Total structural volume may then be calculated from summation of pixel counts of all slices.

Materials and Methods

Digital data were obtained from CT examinations performed with a General Electric 8800 system. Each examination consisted of 30 to 40 adjacent 1.5-mm slices made through a physical phantom and the orbits of a skull phantom and between 25 and 30 slices through the orbits of a normal patient. In the skull phantom and normal patient studies, the axial slices were obtained at 0° to −10° from the orbitomeatal baseline. The patients were encouraged to fix their gaze on focusing points on the overhead gantry during scanning. Small changes in eye direction that occur in all orbit studies likely accounted for part of the measured range of technical error. Patients with obvious misregistration artifacts from eye movements were omitted from the study group. The scan data were then transferred to a Nova 830 stand-alone computer system with Data General drive and Grinnell image display for off-line analysis. Special software programs, as described in a report by Forbes et al. [7], were used to generate pixel counts of prescribed anatomic structures for volume surveys (fig. 1). Region-growing, neighborhood-sampling, and automatic-tracing algorithm techniques were used for boundary display [14]. Pixel counts were summated from all slices and multiplied by a conversion factor (0.00096 cm^3/pixel for the 0.8 × 0.8 × 1.5 mm voxel) for total volume measurement (fig. 2).

The physical phantom was constructed from a cone-shaped plastic cup containing water and pencils to simulate orbital fat and muscle with different density ranges. Numerous scans and volume calculations were obtained with different amounts of water to empirically determine the most favorable density ranges and the counting techniques with the least intrinsic method error and observer variability.

A more realistic phantom was then constructed to simulate an in vivo orbit study (fig. 3). Silicone was used to construct the simulated fat and muscle filling the orbit in a dry skull, and a glass marble was positioned to represent the globe. Irregularly shaped strips, used to represent muscle tissue, were cut from a solid block of pure silicone. The volume of these strips was measured by water displacement (Archimedes principle) before they were attached to the orbital walls in the skull. Iodine-impregnated fluid silicone, representing fat tissue, was poured into the remaining volume of the orbital cavity. After hardening of the iodine-impregnated silicone, the entire mass could be removed for volume measurement. The composite silicone masses were replaced into the skull and scanned with the same CT techniques used for the human studies described below. Display window controls were used to determine upper and lower CT attenuation number bounds of the silicone models between 900 and −100 H. The right phantom orbit was constructed after the left orbit with slightly increased iodine concentration in silicone, which provided improved definition of different material margins. Numerous runs empirically demonstrated the most accurate boundary range settings for densities of the test material. Range settings for the in vivo studies were then based on the densities of the measured structures.

For in vivo analysis, 29 examinations for volume measurements of the orbital soft tissues were performed in 29 normal patients. The study group consisted of 12 women, nine men, five girls, and three boys. Adult status was established at 25 years for complete stabilization of orbitofacial growth. Adult ages ranged from 28 to 76 years; pediatric ages ranged from 6 months to 22 years. All patients were euthyroid without proptosis and generally were referred for orbital CT to evaluate the optic nerves for field cuts and scotomata. Results of all CT imaging examinations were normal in both orbits. Digital data from the CT examination were transferred by tape for the off-line analysis, as described above.

For clinical studies, computed volume measurements were determined for total bony orbit, total orbital soft tissues exclusive of the globe, orbital neuromuscular tissue, and orbital fat. For computer analysis, the bony orbit was defined as the cone-shaped space bounded by the medial and lateral orbital walls, by the orbital roof and floor, and anteriorly by a line from the anterolateral wall to the anteromedial nasal prominence. The ocular muscles were all soft tissues within the soft-tissue-density range exclusive of the optic nerve. The orbital fat was represented by soft tissues below the isodense soft-tissue ranges used for muscle computations.

Results

Measurements were tabulated in three categories: (1) the physical phantom, (2) the dry-skull-and-silicone-orbit phantom, and (3) normal in vivo patient examinations. Data from the first two groups were used to determine levels of precision and accuracy for the technique. The patient study group was used for determination of actual orbital structure volumes.

In the physical phantom, volume calculations of water in the range of 20–50 cm^3 were within 1% of actual water volumes. With small solid structures in the range of 4–10 cm^3

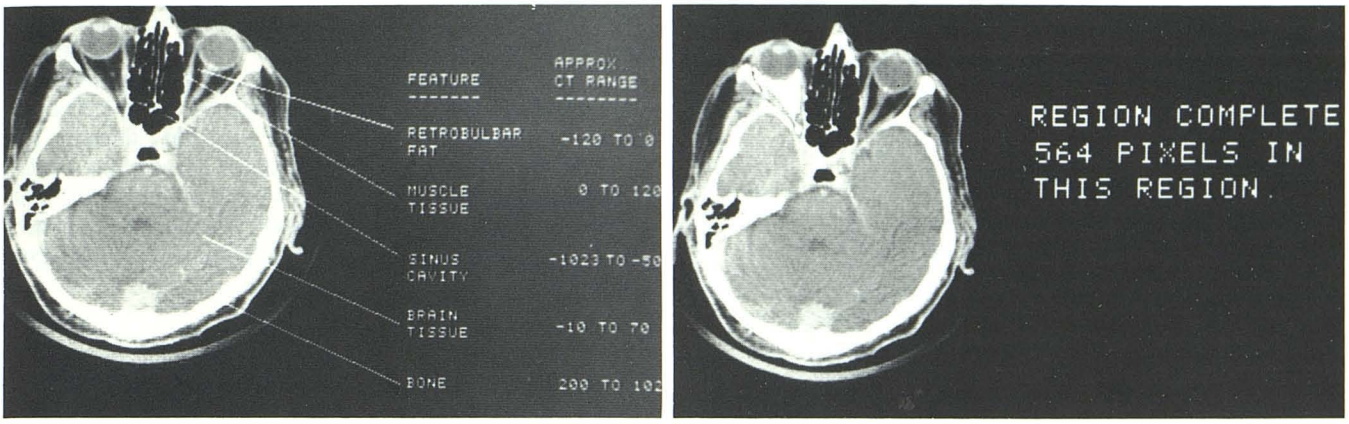

Fig. 2.—**A**, In vivo density range selection. In orbit, wide range of different tissue densities provides good selection of ranges that can be used with minimal overlap. **B**, In vivo pixel counting. Pixels within each specific density range (in this case, intraconal and extraconal fat) are summated in each slice.

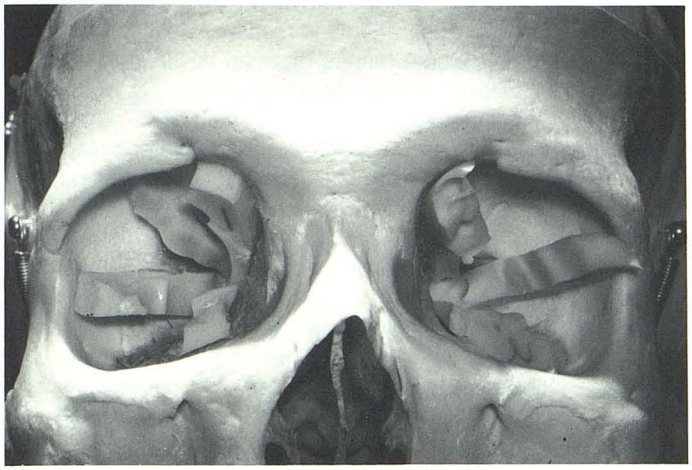

A

B

C

D

Fig. 3.—Skull phantom. **A**, Silicone rubber polymer was used to simulate ocular muscles. Before insertion, rubber muscles were tested for weight, density, and volume. Amorphous shape of polymer phantoms in dry skull provided more precise assessment of computer accuracy for volume measurement. **B**, Iodine-impregnated Silastic originally in liquid form was used to fill rest of bony orbit behind glass eye. Density of this filler was sufficiently different from that of muscles to allow computer separation for pixel counting. **C**, Entire orbital contents are removable as components for volume calibration with water displacement. **D**, Scanning techniques similar to those used in patient studies were applied to measure Silastic orbital contents. Empirical determinations of known Silastic volumes also aided in the establishment of preferred density ranges for each tissue component.

TABLE 1: **Volume Measurements in Orbital Phantom**

Technique	Volume (cm^3)		% Difference*	
	Right	Left	Right	Left
Total orbit:				
Archimedes principle	21.40	21.11	...	...
CT boundary:				
−100–900	22.06	22.70	3.0	7.5
0–825	21.38	21.41	0.0	1.4
100–750	19.88	20.11	−7.1	−4.7
Muscle:				
Archimedes principle	6.00	6.00	...	...
CT boundary:				
−100–350	5.59	5.30	−6.8	−11.6
0–375	6.17	7.20	2.8	20.0
100–350	5.90	6.50	−1.6	8.3
Fat:				
Archimedes principle	15.40	15.11	...	...
CT boundary:				
350–900	15.54	14.37	0.9	−5.0
376–825	13.74	12.20	−10.7	−19.34
351–750	15.90	14.80	3.2	−2.1

* % difference from Archimedes displacement value.

simulating muscle groups, volume calculations were all within 7% of the actual measurements by water displacement. Limitations were due to observer error of boundary margins, overlap of density ranges at the boundaries for tracing algorithms, and partial-volume effects.

Computer calculations from the silicone-orbit-and-dry-skull phantom were compared with water displacement values. Three CT number ranges tested in each structure group resulted in comparative differences of 0%–20%. After empirical testing, boundary ranges properly selected for appropriate structural densities gave volume calculations within 7.5%–8.3% of water displacement values. These ranges are listed in table 1. A proper selection of boundary ranges was important to maintain reproducible results in both phantom and in vivo studies. Ranges were chosen by observation to give the most clearly defined borders between different types of tissue. For the in vivo patient studies, attenuation ranges of −135 H to 0 and 0 to +135 H were used for fat and muscle, respectively, although these attenuation numbers for boundary ranges would likely vary among scanners of different type or manufacture.

For the in vivo patient studies, volume calculations included total bony orbit, total orbital soft tissues exclusive of the globe, neuromuscular soft tissue, and orbital fat. The mean ± 2 SDs was established to arbitrarily define a normal range for subsequent studies of ophthalmopathy. Adult male and adult female values are listed in table 2.

A wider scale in bony orbit volumes in men than in women may have been due to scanning techniques, although this was not apparent from the images. The differences between right and left total bony orbit volumes in all persons were 0.01–1.95 cm^3. Similar differences for fat and muscle measured between right and left orbits in the same person are listed in table 2.

The range of total orbital soft-tissue volume exclusive of the globe in the pediatric orbit was from 5.1 cm^3 in an infant to 13.93 cm^3 in a young adult. Because of the developmental span, there was less immediate significance to the individual volume measurements in the eight pediatric subjects, although relative fat-to-muscle ratios could be compared with those in adults. The ratio of fat to muscle ranged from 1.00 to 1.86, with a mean of 1.54. No trend corresponding to either age or gender was noted in the range of the ratio in the eight pediatric subjects.

Discussion

The soft tissues of the orbit comprise the globe, largely filled with aqueous and vitreous fluid; the muscle groups; small neurovascular structures often adjacent or intertwined with the muscles; the lacrimal gland; and orbital fat. Infiltrative processes, particularly Graves disease, frequently increase the volumes of the muscle and fat compartments [15]. Fortunately, for the purposes of computer analysis, there is significant contrast difference between these anatomic compartments to allow separation and measurement and thus to establish normal volume ranges that can be used for future comparisons with such infiltrative diseases.

With CT volume measurements, the task of CT scanning has been changed from creating images to determining the number of pixels belonging to a predefined density range. Region-growing algorithms have then been used to determine the number of pixels of each category for each slice. The range of CT attenuation values, along with a starting point, is identified for the category of interest. The computer then finds and counts all connected pixels that make up that region, and the process is repeated for all regions of interest from all CT slices. The summation of all pixels for each category when multiplied by a conversion factor represents the estimate of the total.

Although there are variations among individuals, the range of normal adult measurements generally lies within 2 SDs of the mean, an indication of a relatively low variability about the mean. We define the normal adult male bony orbit as one with a volume that can range between 16 and 30 cm^3. The upper limit of normal is 30.1 cm^3, and values above this represent abnormally enlarged orbits. Similarly, the upper limits of normal for orbital soft tissue exclusive of the globe, muscle, and fat are 20.0 cm^3, 6.5 cm^3, and 14.4 cm^3, respectively, when values 2 SDs above the mean are used. We define corresponding values in the women as 17.2 cm^3, 6.2 cm^3, and 12.3 cm^3. The bony and soft-tissue volumes are slightly greater in men as a group than in women.

Volumes of the bony orbit and total orbital soft tissue vary from 0% to 8% between the right and left orbits when measured in the same person. This likely reflects both small anatomic differences and the accuracy of the technique. For the smaller-volume compartments of fat and muscle, the measurable difference between right and left orbits in the same person is 11% and 17%. This in part reflects the greater error related to measurement of very small volumes. Thus, an increase of more than 8% in the volume of the orbital soft

TABLE 2: **Normal Values of Adult Orbital Tissues (42 Orbits)**

Structure	Volume (cm^3)			
	Mean	Range	Mean ± 2 SD	Upper Limit of Normal
Bony orbit:				
Female	23.92	21.58–29.43	...	29.4
Male	23.63	16.18–30.11	...	30.1
Difference (R vs. L)*	0.43	0.01–1.95		8%†
Orbital soft tissues exclusive of globe:				
Female	14.83	12.70–17.30	12.49–17.17	17.2
Male	15.99	12.07–19.25	11.94–20.03	20.0
Difference (R vs. L)*	0.30	0.10–1.29		8%†
Orbital neuromuscular tissue:				
Female	4.69	3.66–6.20	3.19–6.19	6.2
Male	4.79	3.07–6.18	3.10–6.49	6.5
Difference (R vs. L)*	0.01	0.01–0.83		17%†
Orbital fat:				
Female	10.10	8.22–12.20	7.85–12.34	12.3
Male	11.19	8.56–14.00	8.01–14.37	14.4
Difference (R vs. L)*	0.35	0.00–1.30		11%†

* Difference between right orbit measurement and left orbit measurement in the same person for all adults.
† Upper limit of normal variance measured for one orbit compared with the other (in the same subject).

tissues would be necessary to reliably measure unilateral ophthalmopathy in an individual subject. For specific compartments of smaller volume, such as fat and muscle, increases greater than 11% and 17%, respectively, would be necessary to reliably distinguish unilateral ophthalmopathy on the basis of fat or muscle alone.

Certain assumptions are made in establishing these values as normal standards. Tiny neurovascular channels are isodense in CT imaging and thus are averaged into muscle bundles in volume measurements. Because the anterior border of the orbit is open, it is subject to different definitions of boundary. Finally, the values must be considered to have an error of 1%–7%, depending on the relative size of the volume measurement. Nevertheless, these values are uniform within the group and may be used for comparison studies for processes that result in volume changes of orbital fat or muscle.

Various methods to evaluate orbital volumes have been used in the past, including linear measurements, stereoradiography, radiographic tomography, and in vitro dye studies in animals. All previous studies have been limited to bony orbit volumes, dry-skull in vitro determinations, or gross estimates of in vivo bony orbit volume from plain radiographic linear measurements. Linear methods suffer from gross estimates of the irregular polymorphic and slightly ellipsoid shape of the bony orbit, and they led to volumetric determinations of filler materials in dry skulls. In a description of rubber implants for orbit volume studies in rabbits, Sarnat [16, 17] provided an excellent source of review for previous orbital volume methods. Alexander et al. [18] determined bony orbit volumes in human skulls by use of sand, but they found poor correlation with estimated volumes from radiographic measurements. Feldon and Weiner [19] reported linear outline assessment on CT scans to estimate the normal muscle volume in four patients, although neither description of normal ranges in different subjects nor documentation of the accuracy of the technique was provided. Although useful for estimating bony orbit volume, none of these methods could evaluate soft-tissue orbital contents or be used for practical in vivo study of clinical subjects.

Sonography has been used in preliminary studies for both image detection and assessment of the orbital muscles in Graves disease [13]. Yamamoto et al. [20] used B-mode sonography to measure orbital soft-tissue volumes in 31 patients with Graves disease and in six normal controls. Although no phantom studies were performed to establish the accuracy of their technique, the ranges determined for normal and abnormal values were closely similar for both in vivo techniques. In their six normal Japanese controls, single orbital muscle volume had a mean of 3.3 cm^3 ± 1.3 and total bony orbit volume was 24.0–26.7 cm^3. The mean single orbital muscle volume in patients with Graves disease was 6.6 cm^3 ± 2.7. Our own preliminary application of these techniques to patients with this disease showed similar increases distributed over a wide spectrum of clinical variants.

The primary purpose of this work was to establish normal values of orbital structures to serve as a baseline for studies of orbital muscle and fat enlargement. The measurement techniques, however, are universally applicable, with similar CT scanning and off-line processing systems, to other areas of the head and body. The collimated 1.5-mm slices have been measured in our institution to produce an overall entrance dose of 3.5 R to the eye, which is in an acceptable range for an orbital CT scan whether obtained by direct axial and direct coronal or thin-section axial and reformatting techniques [21]. Signals generated from other sources, such as magnetic resonance imaging, may be similarly used for graphic display and volume measurement. A principal advantage of the computer scanning systems lies in avoiding geometric magnification for accurate measurement. Limits of resolution and accuracy are based largely on the size of the measured object related to slice thickness. Differences in

contrast are necessary to discriminate the measured object from surrounding tissue for clinical in vivo studies. These techniques may provide a useful tool in a multitude of situations involving volume considerations as part of a pathologic process.

ACKNOWLEDGMENTS

We thank A. Bennett Reeves, maxillofacial prosthetist, Department of Dentistry, Mayo Clinic, for aid in preparing the orbit phantom and Gerald McGrath, Section of Medical Pathology, Mayo Clinic, for aid in phantom volume measurement with Archimedes principle.

REFERENCES

1. Levi C, Gray JE, McCullough EC, Hattery RR. The unreliability of CT numbers as absolute values. *AJR* **1982**;139:443–447
2. Rhodes ML. Towards fast edge detection for clinical 3-D applications of computer tomography. In: *Proceedings of the Sixth Conference on Computer Applications in Radiographic and Anatomical Radiology Images*. Newport Beach, CA: Institute of Electrical and Electronic Engineers, **1979**:321–327
3. Rosenfeld A, Kak AC. *Digital picture processing.* New York: Academic, **1976**
4. Brenner DE, Whitley NO, Houk TL, Aisner J, Wiernik P, Whitley J. Volume determinations in computed tomography. *JAMA* **1982**;247:1299–1302
5. Heymsfield SB, Fulenwider T, Nordlinger B, Barlow R, Sones P, Kutner M. Accurate measurement of liver, kidney, and spleen volume and mass by computerized axial tomography. *Ann Intern Med* **1979**;90:185–187
6. Moss AA, Friedman MA, Brito AC. Determination of liver, kidney, and spleen volumes by computed tomography: an experimental study in dogs. *J Comput Assist Tomogr* **1981**;5:12–14
7. Forbes G, Gorman CA, Gehring D, Baker HL Jr. Computer analysis of orbital fat and muscle volumes in Graves ophthalmopathy. *AJNR* **1983**;4:737–740
8. Riley FC. Orbital pathology in Graves' disease. *Mayo Clin Proc* **1972**;47:975–979
9. Solomon DH, Chopra IJ, Chopra U, Smith FJ. Identification of subgroups of euthyroid Graves's ophthalmopathy. *N Engl J Med* **1977**;296:181–186
10. Trokel SL, Hilal SK. Recognition and differential diagnosis of enlarged extraocular muscles in computed tomography. *Am J Ophthalmol* **1979**;87:503–512
11. Trokel SL, Jakobiec FA. Correlation of CT scanning and pathologic features of ophthalmic Graves' disease. *Ophthalmology* **1981**;88:553–564
12. Werner SC. Classification of the eye changes of Graves' disease (editorial). *J Clin Endocrinol Metab* **1969**;29:982–984
13. Werner SC. Modification of the classification of the eye changes of Graves' disease: recommendation of the Ad Hoc Committee of the American Thyroid Association (editorial). *J Clin Endocrinol Metab* **1977**;44:203–204
14. Keller JM, Edwards FM, Rundle R. Automatic outlining of regions on CT scans. *J Comput Assist Tomogr* **1981**;5:240–245
15. Forbes G. Computed tomography of the orbit. *Radiol Clin North Am* **1982**;20:37–49
16. Sarnat BG. The orbit and eye: experiments on volume in young and adult rabbits. *Acta Ophthalmol [Suppl]* (Copenh) **1981**;147:1–44
17. Sarnat BG. Orbital volume in young and adult rabbits. *Anat Embryol* (Berl) **1980**;159:211–221
18. Alexander JCC, Anderson JE, Hill JC, Wortzman G. The determination of orbital volume. *Can J Ophthalmol* **1961**;24:105–111
19. Feldon SE, Weiner JH. Clinical significance of extraocular muscle volumes in Graves' ophthalmopathy: a quantitative computed tomography study. *Arch Ophthalmol* **1982**;100:1266–1269
20. Yamamoto K, Itoh K, Yoshida S, et al. A quantitative analysis of orbital soft tissue in Graves' disease based on B-mode ultrasonography. *Endocrinol Jpn* **1979**;26:255–261
21. Forbes GS, Earnest F IV, Waller RR. Computed tomography of orbital tumors, including late-generation scanning techniques. *Radiology* **1982**;142:387–394